The Cryosphere Discuss., doi:10.5194/tc-2015-233, 2016
Manuscript under review for journal The Cryosphere
Published: 26 January 2016

The Cryosphere Discussions
Open Access
EGU

Sea ice diffusion in the Arctic ice pack: a comparison between observed buoy trajectories and the neXtSIM and TOPAZ-CICE sea ice models

Pierre Rampal[1], Sylvain Bouillon[1], Jon Bergh[1], and Einar Olason[1]

[1]Nansen Environmental and Remote Sensing Center and Bjerknes Centre for Climate Research, Thormøhlens gate 47, 5006 Bergen, Norway

Correspondence to: Pierre Rampal (pierre.rampal@nersc.no)

Abstract. Due to the increasing activity in Arctic, sea ice-ocean models are now frequently used to produce operational forecasts, for oil spill trajectory modelling and to assist in offshore operations planning. In this study we propose a method based on a Lagrangian diffusion analysis to evaluate the sea ice drift properties simulated by two sea ice models, TOPAZ-CICE and neXtSIM, used in two different sea ice-ocean systems developed for such applications. We compare their results to the buoy trajectories of the International Arctic buoy Program (IABP) data set and we find that neXtSIM performs better than TOPAZ-CICE in simulating the mean and fluctuating sea ice velocities over the central Arctic in winter. Our analyses indicate that both TOPAZ-CICE and neXtSIM are able to simulate two distinct sea ice diffusion regimes depending on the time scale considered, similarly to what is predicted by the steady and homogenous turbulent flow theory. However, the basin-averaged absolute diffusion computed from the analysis of drifters trajectories simulated with TOPAZ-CICE is almost twice as high as the value estimated from both the corresponding drifters trajectories simulated with neXtSIM and from observed buoy trajectories. Also, the mean Arctic pattern of absolute diffusion obtained from TOPAZ-CICE shows large differences from the one obtained from the observed buoy trajectories, while the neXtSIM results are much more consistent with the results from the buoy trajectories. The information on the mean drift and diffusivity fields provided by our analysis can be used in an advection/diffusion equation or with Lagrangian passive tracers models to study the drift of e.g. pollutants or micro-organisms moving with the ice. More generally, the analysis presented in this paper should be seen as a useful evaluation metric of coupled sea ice-ocean models that aim at being used in operational forecasting platforms, for process and climate studies.

The Cryosphere Discuss., doi:10.5194/tc-2015-233, 2016
Manuscript under review for journal The Cryosphere
Published: 26 January 2016

1 Introduction

The main goal of the present study is to evaluate the sea ice velocity fields provided by two sea ice models that are currently used to produce operational forecast and to simulate pollutant spread in ice-covered areas. A secondary objective is to provide accurate information on specific statistical properties of sea ice motion that could be used to better assess the predictability of the ice trajectories, hence improving the evaluation of their uncertainty.

In order to state the problem, it is interesting to get back to the review of Drozdowski et al. (2011) on oil spill trajectory modelling in the presence of sea ice, in which they made the following statement: "The comprehensive oil spill trajectory modelling system can be expected to provide reliable short term predictions, perhaps for several days to a week. However a spill that occurs in the fall may be inaccessible for 6 or more months. The picture for oil spill trajectory modelling for the long term, say 6 months, is less clear. The multiple pathways for oil movement and the uncertainty in the ocean currents, sea ice drift and the oil-ice interactions means that deterministic model predictions (i.e. a definite prediction of where the oil will go) become unreliable, and that probabilistic predictions (i.e. the model assigns probabilities that the oil will be found at any particular location) are required. The key point is that any ice-ocean model used for the oil spill trajectory modelling needs to provide a credible representation of the large scale spatial variability in the ocean currents and the sea ice drift in addition to the storm driven variability."

An interesting research task is to investigate what is the regime of diffusion of a pollutant trapped in sea ice. To do so, one can separate the deterministic from the non-deterministic part of the sea ice motion within the theoretical framework developed for turbulent diffusion in fluids. Indeed, previous studies showed that turbulent theory may be applied to study diffusion properties of sea ice (Lukovich et al., 2011, 2015; Rampal et al., 2009b; Thorndike, 1986; Colony and Thorndike, 1985). Following the turbulent theory of Taylor (1921), Thorndike (1986) were able to split sea ice motion into a predictable mean part, $\bar{u}$, and a random fluctuating part, u'. The predictable part is forced by the large scale mean motions in the atmosphere and the ocean, while the random part was suggested by Thorndike (1986) to be forced by short term fluctuations in the wind and ocean currents. Later, Rampal et al. (2009b) showed that the fluctuating part of the sea ice motion is also influenced by the mechanical response of the sea ice cover itself, and presented a method based on the turbulent theory of Taylor (1921) to extract this fluctuating part from the total motion. Note that similar methodology has been applied to study diffusion properties from Lagrangian drifters in the ocean (see e.g., Zhang et al., 2001; Poulain and Niiler, 1989). With this method it is possible to study the characteristics of the sea ice motion in a statistical sense, for different conditions and seasons.

In this study we analyse the quality of the sea ice motion fields provided by the TOPAZ-CICE (hereafter referred as TOPAZ) and neXtSIM sea ice models by comparing synthetic buoy trajectories simulated by the models to the corresponding buoy trajectories of the International Arctic buoy Program (IABP) data set. The statistical properties of these trajectories are analysed to evaluate how

The Cryosphere Discuss., doi:10.5194/tc-2015-233, 2016
Manuscript under review for journal The Cryosphere
Published: 26 January 2016

the mean drift field and the fluctuating part of the sea ice motion are reproduced by the models. The IABP buoy data set that was used by Rampal et al. (2009b, 2008) covers the period 1979-2011, but the analysis presented in this paper is restricted to winter conditions. In this study the comparison against the measured IABP data is performed for the years 2007 to 2010 during which the spatial and temporal coverage of the IABP buoys is relatively good, i.e. with more than 40 buoys active every day, allowing for higher statistical significance in comparisons.

This paper is organised as follows: the different data sets are presented in Section 2, the methods used for the analysis are presented in Section 3 and the results for the diffusion analysis in Section 4. The link with passive tracer trajectory modelling is discussed in Appendix A and we finalise the article with a discussion, a conclusion, and a description of future work.

The Cryosphere Discuss., doi:10.5194/tc-2015-233, 2016
Manuscript under review for journal The Cryosphere
Published: 26 January 2016

2 Data

We use the full 12-hourly buoy positions from the International Arctic Buoy Program data set for the 1979-2011 period as a reference (Rigor, I. G. Compiled by Polar Science Center. 2002. IABP Drifting Buoy Pressure, Temperature, Position, and Interpolated Ice Velocity, Version 1. subset C. Boulder, Colorado USA. NSIDC: National Snow and Ice Data Center. http://dx.doi.org/10.7265/N53X84K7. January 2015). For the period 2007 to 2010 we also generate “virtual" buoy trajectories by putting floats in the TOPAZ and neXtSIM models. The floats are initialised at the same time and position as the IABP buoys, and are “killed" when the IABP buoy track stops or when the virtual buoy enters into an area of simulated open water (sea ice concentrations less than 15%). After removing the few non-overlapping periods (i.e. the periods for which the trajectories are not available in the three data sets), three comparable data sets are obtained: i) the observed sea ice trajectories, ii) the trajectories of virtual sea ice floats simulated by TOPAZ, and iii) the trajectories of virtual sea ice floats simulated by neXtSIM. Because the buoy positions of the IABP dataset are sampled every 12 hours, the virtual TOPAZ and neXtSIM float trajectories originally sampled every hour are sub-sampled to obtain 12-hourly positions as well.

We increased the number of buoy trajectories by splitting the buoy trajectories longer than 35 days into as many segments of 35 days as possible, the remaining data being discarded. Since we know that the memory of a piece of ice of its past motion is less than 10 days (Rampal et al., 2009b), each of these 35-days buoy track segments can be assumed to be independent from the others. When removing non-overlapping segments in the three data sets, we are left with 280 individual floats and 3720 35-day segments in each data set for the period 2007 to 2010.

A polar stereographic projection is used to change the IABP and Virtual buoy positions from geographic (lat, lon) coordinates to Cartesian (x, y) coordinates in km from the north pole. Velocities are then calculated along each buoy track as

$$u\left(\tilde{x},\tilde{t}\right) = \left(x\left(t+\Delta t\right) - x\left(t\right)\right)/\Delta t \quad (1)$$

$$v\left(\tilde{y},\tilde{t}\right) = \left(y\left(t+\Delta t\right) - y\left(t\right)\right)/\Delta t \quad (2)$$

at positions $\tilde{x} = (x(t+\Delta t) + x(t))/2$, $\tilde{y} = (y(t+\Delta t) + y(t))/2$ and time $\tilde{t} = t + \Delta t/2$. The time step, Δt is 12h for the IABP data and for the virtual buoys.

2.1 IABP

Originally, the raw IABP buoy positions were sampled irregularly in time with a mean time interval of 1 hour, and with errors ranging from 100 to 300 m depending on the position system (Thomas, 1999). Before being delivered to the scientific community, the buoy positions were interpolated (using a cubic function) to form an homogeneous trajectory data set giving for each buoy its position every 12 hours.

The Cryosphere Discuss., doi:10.5194/tc-2015-233, 2016
Manuscript under review for journal The Cryosphere
Published: 26 January 2016

To investigate sea ice motion properties in the pack ice, we restricted the IABP dataset to a region located in the centre of the Arctic basin (hereafter denoted the Central Arctic domain), i.e. above 70 N, at least at 100 km from the nearest coast and from the section of the 80^{th} parallel going from Greenland to Severnaya Zemlya. Sea ice dynamics in coastal regions are specific with for example the presence of land-fast ice and would require a dedicated study. We also restrict the analysis to the winter period defined as starting the 1^{st} of November and ending the 15^{th} of May. Each individual buoy track from the IABP dataset has been checked manually to clean them from unrealistic “jumps" or "spikes" in the trajectories, or when the dating system was giving obviously wrong times. These unrealistic “jumps" are due to errors in the positioning system embarked on the buoy or in the recordings during the deployment or recovering of the instruments. The period 2007-2010 has been selected for its relatively good coverage, with more than 40 buoys recording their positions simultaneously every day. Buoy trajectories shorter than 30 days have been removed.

Figure 1 shows all the trajectories analysed in this study. The IABP data set from 1979 to 2011 covers almost the whole Central Arctic domain except the East Siberian and Laptev Seas. The different data sets for the period 2007 to 2010 (i.e. the one from IABP and the two generated from model simulations) are much sparser and cover a smaller portion of the Arctic Ocean. As shown in the Figure 1, these trajectories are rather complex geometrically, e.g. with abrupt changes in the direction.

2.2 Float tracks generated with the TOPAZ model

The forecast system TOPAZ is the official Arctic Ocean forecast platform of the European Copernicus Marine Environment Monitoring service (http://marine.copernicus.eu). The ocean part of TOPAZ uses HYCOM version 2.2, with 28 vertical layers divided into isopycnal layers in the stratified interior of the open ocean and z-coordinates in the unstratified surface mixed layer (Bleck, 2002). The ocean model is coupled to a one thickness category sea ice model based on CICE, the Los Alamos Sea Ice Model, version 4 (Hunke and Lipscomb, 2010). The part that solves the sea ice dynamics is built around a standard EVP rheology (Hunke and Dukowicz, 1997) while the one solving sea ice thermodynamics is described in Drange and Simonsen (1996). The sea ice strength is set to 27 500 N and the advection of sea ice scalar variables is calculated using a 3^{rd} order WENO scheme (Jiang and Shu, 1995) with a 2^{nd} order Runge-Kutta time discretisation. The sea ice-ocean model is run here in free-run mode (i.e., no data assimilation is applied). The model is initialised from a restart file taken from the free-run simulation described in Sakov et al. (2012). The TOPAZ coupled sea ice-ocean system provides sea ice variables, such as sea ice velocities, concentration, and thickness, at a high temporal resolution (i.e. every hour). A more detailed description of the TOPAZ system may be found in Sakov et al. (2012).

The applied atmospheric forcing fields are the 6-hourly 10-meter wind velocities from the ERA interim reanalysis (ERAi) distributed at 80 km spatial resolution (http://www.ecmwf.int/en/research/

The Cryosphere Discuss., doi:10.5194/tc-2015-233, 2016
Manuscript under review for journal The Cryosphere
Published: 26 January 2016

climate-reanalysis/era-interim, ECMWF (2011)). The frictional drag parameters for the atmosphere-ice stress ($c_a = 0.0016$) and for the ice-ocean stress ($c_w = 0.0055$) are those currently used and optimised for the TOPAZ operational platform.

The float tracking with TOPAZ is performed off-line. Hourly sea ice motion simulated by the model is used to force the off-line float tracking system that moves the floats in the quasi-homogeneous TOPAZ Arctic grid. We use that grid instead of a regular longitude/latitude grid in order to avoid singularity errors at and around the Pole. The advantage of the off-line float tracking system is that it allows us to easily perform experiments for a given time period and location and with a reasonably large number of floats. We checked that for the time scale and spatial resolution considered here, this off-line tracking method is giving similar results to using an online tracking system, while remaining computationally efficient.

The float-tracking system initialises floats at a prescribed start position (longitude and latitude) and starting time (year, month, day and hour), then moves the floats with a simple Eulerian method and kills the floats at a prescribed end time (year, month, day and hour) so that it matches the end of the corresponding real IABP buoy's trajectories. The Eulerian sea ice velocities given by the TOPAZ model are interpolated to the position of the virtual Lagrangian floats every hour. Floats drifting out of the simulated sea ice cover, i.e. where sea ice concentration is below 15% in the present case, are not tracked further. The virtual buoy tracks are stored as longitude and latitude positions.

2.3 Float tracks generated with the neXtSIM model

neXtSIM is a fully-Lagrangian thermodynamic-dynamic sea ice model, using an adaptive finite element mesh and a mechanical framework based on the elasto-brittle rheology (Rampal et al., 2015). The domain used for the simulations with the neXtSIM model is defined from TOPAZ (version 4) coastlines and open boundaries. It covers the Arctic and North-Atlantic Oceans, extending from an open boundary at 43°N in the North-Atlantic to an open boundary in the Bering Strait. The mean resolution of the finite element mesh used by neXtSIM is about 10 km. Thermodynamic growth and melt of the ice are based on Semtner (1976) and the ice model is coupled to a slab ocean model. The temperature and salinity in the slab ocean model are constantly nudged towards values of the TOPAZ reanalysis in order to simulate oceanic heat and salt transfer. A complete description of this stand-alone version of the neXtSIM sea ice model as well as his coupling to the slab ocean model may be found in Rampal et al. (2015).

The neXtSIM model is able to simulate the observed evolution of the sea ice volume, extent and area over an annual time scale (Rampal et al., 2015). However, the simulated drift and deformation fields have only been extensively evaluated for the winter season in Rampal et al. (2015) and Bouillon and Rampal (2015). The three simulations used for this study are therefore starting on September 15^{th} and finishing on May 15^{th} 2007, 2008 and 2009, and our analysis is restricted to winter time, i.e. from November to May. The model is initialised with the ice concentration derived from the

The Cryosphere Discuss., doi:10.5194/tc-2015-233, 2016
Manuscript under review for journal The Cryosphere
Published: 26 January 2016

AMSR-E passive microwave sensor (Kaleschke et al., 2001; Spreen et al., 2008, data obtained from the Integrated Climate Date Center, University of Hamburg, Germany, http://icdc.zmaw.de) and the TOPAZ ice thickness, within the area reported by AMSR-E as being covered with ice. The modelled ice thickness of the TOPAZ model is known to be biased (too low) and so we increase the initial thickness uniformly so that the total volume is the same as that given by the PIOMAS model on September 15^{th} 2007, 2008 and 2009 (Zhang and Rothrock, 2003). The good performance of PIOMAS in simulating Arctic sea ice volume as compared to available observations is reported in Schweiger et al. (2011). The temperature and salinity of the slab ocean model are initialised with temperature and salinity from TOPAZ.

The model is forced with the ocean state of the TOPAZ4 reanalysis (see Sakov et al., 2012). The oceanic forcing variables are sea surface height, velocity at 30 m depth, and sea surface temperature and salinity (for more details, see Rampal et al. (2015)). The atmospheric state comes from the Arctic System Reanalysis, Interim version (ASR-Interim hereafter) (http://rda.ucar.edu/datasets/ds631.4/, Byrd Polar Research Centre/The Ohio State University (2012). Accessed 01 Jan 2014). The ASR-Interim is a high resolution atmospheric reanalysis (30 km) known to reproduce particularly well the near-surface wind fields in the Arctic region (Bromwich et al., 2015).

The frictional drag parameter for the atmosphere-ice boundary layer is closely linked to the applied atmospheric forcing field and directly impacts sea ice motion. The common approach to optimise this parameter is to compare the simulated and observed sea ice drift over the whole Arctic basin. However, this approach leads to interdependence between the optimisation of the mechanical parameters and the optimisation of the air drag coefficient. Instead, we developed a tuning methodology that has the advantage of differentiating the choice of the air drag coefficient from the mechanical parameters. This method and its results are presented in Rampal et al. (2015). We here use the values for the air drag parameter ($c_a = 0.0076$) found to be optimal when using the ASR wind forcing and the same value of water drag parameter as in TOPAZ ($c_w = 0.0055$)

The float tracking with neXtSIM is performed at run time. The main reason for doing this is that the Lagrangian advection used in the neXtSIM model offers some additional challenges to a post-processing approach over the Eulerian advection used in TOPAZ. Using this approach, the tracking system is initialised with floats that have the same positions and starting dates as the IABP buoys. These positions then change as the underlying mesh moves and are interpolated onto the new mesh after each remeshing step. (See Rampal et al. (2015) for more details on the remeshing procedure.) The virtual drifters are removed when the corresponding IABP buoy tracks stop or when the simulated local ice concentration falls below 15%. The procedure of adding and removing buoys is therefore the same as the one followed for the aforementioned off-line float tracking system used with TOPAZ.

The Cryosphere Discuss., doi:10.5194/tc-2015-233, 2016
Manuscript under review for journal The Cryosphere
Published: 26 January 2016

3 Methods

The method used to analyse the Lagrangian particles/floats obtained from IABP, TOPAZ and neXtSIM is similar to the one presented in Rampal et al. (2009b) and is based on the theory proposed by Taylor (1921) to study turbulent fluid. For the decomposition of the motion into a mean and a fluctuating part, we follow the classical approach used to study Lagrangian trajectories (see for example Zhang et al., 2001).

3.1 Diffusion theory of Taylor (1921)

Following the theory developed for turbulent fluids by Taylor (1921), diffusion describes in a statistical sense how an individual particle moves apart from any of its previous position. Taylor's diffusion theory is valid for steady and homogeneous turbulent flow without mean flow and for which the fluctuating velocity follows a Gaussian distribution. When following a single particle in such conditions, the variance of its fluctuating displacement $\langle r'^2(t)\rangle$ should in theory evolves as

$$\langle r'^2(t)\rangle = 2\langle u'^2\rangle \int_0^t \int_0^{t_1} C(\tau) d\tau dt_1 \tag{3}$$

where $\langle u'^2\rangle$, the variance of the fluctuating velocity, is constant in time and $C(\tau)$, the Lagrangian normalized autocorrelation function, is defined as

$$C(\tau) = \frac{1}{\langle u'^2\rangle T_{\max}} \int_0^{T_{\max}} \mathbf{u}'(t)\mathbf{u}'(t+\tau) dt. \tag{4}$$

where $T_{\max}$ is the duration of the particle trajectory (here 35 days) and $\mathbf{u}'(t)$ is its fluctuating velocity at time t defined following the method described in Section 3.2.

For very long time intervals τ, the autocorrelation vanishes and the integral of $C(\tau)$

$$\Gamma = \int_0^{\infty} C(\tau) d\tau. \tag{5}$$

is then a constant. This constant Γ is referred as the Lagrangian integral time scale and determines the transition between two diffusion regimes. For time much shorter than Γ, we are in the "ballistic" regime and Equation 3 becomes

$$\langle r'^2(t)\rangle = \langle u'^2\rangle t^2, \qquad t << \Gamma, \tag{6}$$

(this simply comes from the fact that $C(\tau)$ tends to the limiting value unity for small t). For time much longer than Γ, we are in the "Brownian" regime (also called "random walk" regime) and Equation 3 becomes

$$\langle r'^2(t)\rangle = 2\langle u'^2\rangle \Gamma t + \alpha, \qquad t >> \Gamma, \tag{7}$$

The Cryosphere Discuss., doi:10.5194/tc-2015-233, 2016
Manuscript under review for journal The Cryosphere
Published: 26 January 2016

where α is a constant defined as $\alpha = -2\int_0^\infty \tau C(\tau)d\tau$ (LaCasce, 2008). The second regime is similar to the one driven by molecular diffusion (i.e., where fluctuating velocities are also uncorrelated) but with much larger diffusion coefficients.

Following Lagrangian turbulent theory, diffusivity (noted K) is defined as follows:

$$K = \frac{1}{2}\frac{d\langle r'^2(t)\rangle}{dt}. \tag{8}$$

In the “ballistic" regime (with Equation 6), diffusivity increases with time and may be calculated as

$$K = \langle u'^2\rangle t. \tag{9}$$

In the “Brownian" regime (with Equation 7), diffusivity (also called absolute diffusivity in that case) is constant and may be calculated as

$$K = \langle u'^2\rangle \Gamma. \tag{10}$$

In the present study we will use the absolute diffusivity to compare the different data sets.

3.2 Decomposition of the sea ice motion

As shown in the previous section, one may look at statistical properties of fluctuating displacements to study diffusion properties. Therefore, we need to decompose the total sea ice motion into a mean and a fluctuating part. We here shortly describe how this decomposition is performed and how the fluctuating part of the motion is then described. A more complete and detailed presentation of the methodology, in particular of how to choose the appropriate temporal and spatial averaging scales, can be found in Rampal et al. (2009b).

3.2.1 Mean velocity calculation

From the list of positions $\mathbf{x}_q^i$ of a buoy q given with a regular time interval Δt, one can evaluate its position and velocity at time $t = t_q^i + 0.5\Delta t$ by computing:

$$\mathbf{x}_q(t) = \left(\mathbf{x}_q^{i+1} + \mathbf{x}_q^i\right)/2, \tag{11}$$

$$\mathbf{u}_q(t) = \left(\mathbf{x}_q^{i+1} - \mathbf{x}_q^i\right)/\Delta t. \tag{12}$$

By doing the same for all the available buoys, one can build a data set recording all the velocities computed at a time scale Δt.

From that data set a mean velocity field $\bar{\mathbf{u}}_{L,T}(\mathbf{x},t)$ can be defined for a given spatial and temporal scale, L and T, by averaging all the buoy velocities $\mathbf{u}_k$ recorded at a distance less than $L/2$ from $\mathbf{x}$ and within the time window $[t - T/2; t + T/2]$. The averaging operator used here is

$$\bar{\mathbf{u}}_{L,T}(\mathbf{x},t) = \frac{1}{\sum_k w_k}\sum_k w_k \mathbf{u}_k, \tag{13}$$

where w_k are the weight coefficients defined as

$$w_k = e^{\left(-\frac{r_k^2}{2L^2} - \frac{\tau_k^2}{2T^2}\right)} \quad \text{with } r_k = \sqrt{(x_k - x)^2 + (y_k - y)^2} \quad \text{and } \tau = t_k - t. \tag{14}$$

The Cryosphere Discuss., doi:10.5194/tc-2015-233, 2016
Manuscript under review for journal The Cryosphere
Published: 26 January 2016

This mean velocity is then evaluated at each recorded position $\mathbf{x}_q(t)$ and subtracted from the recorded velocities to define the fluctuating velocities by computing

$$\mathbf{u}'_q(t) = \mathbf{u}_q(t) - \bar{\mathbf{u}}_{L,T}(\mathbf{x}_q(t), t). \tag{15}$$

As seen in Equation 15, the fluctuating velocities depend on the value of the averaging scales, L and T. This dependance and the fact that the autocorrelation function has to remain close to 0 for long time interval τ provide an elegant method to determine the appropriate value for L and T. First we compute for each buoy trajectory q and pair of averaging scales L and T, the normalized autocorrelation function, $C_q^{L,T}$, using Equation 4. Secondly, we calculate an ensemble average autocorrelation function as

$$\chi^{L,T}(\tau) = \frac{1}{\sum_q T^q_{\max}} \sum_q T^q_{\max} C_q^{L,T}(\tau) \tag{16}$$

where the influence of each buoy is weighted by the time length of its trajectory, $T^q_{\max}$. Finally, we select the averaging scales for which $\chi^{L,T}(\tau)$ remains close to 0 for large τ. An example of $\chi^{L,T}(\tau)$ function obtained with $L = 400$ km and $T = 165$ days is presented in Figure 2. The results of this analysis are detailed and discussed in Section 4.

An equivalent method to the one described above is to define the appropriate spatial and temporal averaging scales as the lowest scales for which $\Gamma^{L,T}$ remains quasi constant (i.e., less than 1% change). Since we cannot integrate Equation 5 to infinity, the average integral time scale $\Gamma^{L,T}$ for the selected period is computed as

$$\Gamma^{L,T} = \int_0^{t_0} \chi^{L,T}(\tau) d\tau \tag{17}$$

where t_0 is the first time $\chi^{L,T}(\tau)$ crosses zero (see for instance Poulain and Niiler, 1989; Rampal et al., 2009b). In the example of Figure 2, $t_0 = 6$ days and the integration time scale Γ for $L = 400$ km and $T = 165$ days is equal to 1.5 days. Note that the absolute diffusivity ($K = 1.0 \times 10^3\,\mathrm{m^2\,s^{-1}}$) for the example of Figure 2 is also given for information but will be discussed in Section 4. We verified by plotting $\Gamma^{L,T}$ (not shown) that a plateau is reached for averaging scales larger than $L = 400$ km and $T = 165$ days, which is then the appropriate averaging scale for the example shown here.

The Cryosphere Discuss., doi:10.5194/tc-2015-233, 2016
Manuscript under review for journal The Cryosphere
Published: 26 January 2016

4 Results

The result of the diffusion analysis applied to the whole IABP data set from 1979 to 2011 is used as a reference to get an overall picture for the Central Arctic region. In addition, we present a comparison between observed and simulated float trajectories for the winter seasons 2007 to 2010. We restrict our analysis here to winter seasons because of the too sparse buoy trajectories available in the IABP dataset during summer, and because the performance of the neXtSIM model has been extensively assessed so far for winter only (Rampal et al., 2015).

Figure 3 shows the maps with all the buoy trajectories for each winter season from the IABP data set, the TOPAZ model and the neXtSIM model. From this figure, we can already see that the trajectories from the neXtSIM model are more similar to observations than the ones from the TOPAZ model. We clearly see that, in general, the TOPAZ trajectories are longer than their corresponding ones in the IABP data set. The short IABP trajectories north of the Canadian Arctic Archipelago (clearly seen in 2007/2008 winter) are the result of the significantly thicker and more ridged sea ice, which leads to nearly zero speed in that region. This dynamical sea ice response, i.e. the expected drift behaviour of a solid thick plate of ice surrounded by closed boundaries and stressed by external forces, is captured by neXtSIM but not by TOPAZ. To better describe the differences between the simulated and observed trajectories, we analyse separately the mean drift and the fluctuating part of the motion by applying the so-called Taylor's decomposition to the sea ice velocities.

4.1 Decomposition of the sea ice motion

To compute the mean part of the motion, Rampal et al. (2009b) determined that the appropriate averaging scales to be used for the entire IABP data set are $L = 400$ km and $T = 5.5$ months (165 days) for winter, and $L = 200$ km and $T = 2.5$ months for summer. These spatial and temporal averaging scales are defined as the smallest values for which the integral time $\Gamma^{L,T}$ remains quasi constant. By performing a similar analysis as in Rampal et al. (2009b) for the IABP data but only from 2007 to 2010, we found that the same averaging scales should be used and so we did to compute the mean part of the motion at each location of buoy along their track in the present study.

Applying the averaging scales $L = 400$ km and $T = 165$ days with the procedure described in section 3.2.1, we split the velocity field into a mean, $\bar{\mathbf{u}}$, and a fluctuating part, $\mathbf{u}'$. The fluctuating sea ice displacement is then derived from the fluctuating velocities as

$$\begin{aligned} r'_x(t) &= r'_x(t-\Delta t) + u'(t)\Delta t \\ r'_y(t) &= r'_y(t-\Delta t) + v'(t)\Delta t, \end{aligned} \tag{18}$$

with $r'_x(t=0) = 0$ and $r'_y(t=0) = 0$ and where Δt is the time step in the data set.

Figure 4 shows an example of the partition of the displacement of an IABP buoy into its mean and fluctuation trajectories. With this partitioning method, the mean motion can be considered homogeneous and stationary at temporal and spatial scales smaller or equal to T and L, whereas the

The Cryosphere Discuss., doi:10.5194/tc-2015-233, 2016
Manuscript under review for journal The Cryosphere
Published: 26 January 2016

fluctuating motion contains the unpredictable part linked to turbulent and small scale motion. The loops in the fluctuation trajectory seen on Figure 4 are typical small scale motion features and shall be related to the response of sea ice to local and non-stationary oceanic eddies and atmospheric perturbations.

4.2 Mean velocity field

The mean velocity fields for each winter season and for the three data sets, i.e. IABP, TOPAZ and neXtSIM, are shown in Figure 5. Unsurprisingly, the two main features in the mean Arctic-wide sea ice circulation computed with our method are the Beaufort Gyre and the Transpolar drift. However, we note that the strength and the size of the Beaufort Gyre, as well as the strength of the Transpolar drift, vary from one year to the other. This inter-annual variability is well represented by both TOPAZ and neXtSIM. The two models, however, perform differently in terms of the magnitude and the spatial distribution of the mean sea ice drift. The TOPAZ model generally overestimates the mean field and does not correctly reproduce the spatial patterns. In particular the size of the Beaufort Gyre is often overestimated and the model does not reproduce the low velocities in the “lower" part of the Beaufort Gyre, along the Canadian Arctic Archipelago (see, for example, the first line of Figure 5). The mean ice drift simulated by the neXtSIM model is much more similar to the observations in that respect. Indeed, it better reproduces the patterns and intensity of the mean ice drift in the Beaufort Sea, Eurasian basin and along the Canadian Arctic Archipelago where the ice is almost immobile according to the observations.

The statistical distribution of the mean velocity also gives valuable information and can be used to evaluate the output of sea ice models. Figure 6 shows the probability density function of the mean speed (i.e., the norm of the mean velocities), $\bar{U} = \sqrt{\bar{u}^2 + \bar{v}^2}$, as computed from the IABP buoy data and from the TOPAZ and neXtSIM virtual buoy data for the period 2007-2010. The mean speed distribution from the observations fits well with an exponential function. The exponential distribution has the peculiarity of being fully determined by the mean value, which is also equal to the standard deviation. In the case of the IABP data, the mean value of the mean drift is equal to $2.45\,\mathrm{cm\,s^{-1}}$. The same analysis performed on the two models indicates that TOPAZ produces mean velocities following a Gaussian distribution instead of an exponential distribution with a mean of the distribution equal to $3.38\,\mathrm{cm\,s^{-1}}$. The mean velocities simulated by the neXtSIM model follow an exponential distribution with a mean equal to $2.00\,\mathrm{cm\,s^{-1}}$, slightly lower than the observations. We conclude that the TOPAZ model overestimates the mean ice drift by about 38%, whereas neXtSIM underestimates the mean drift by about 18%.

4.3 Fluctuating velocity field

When removing the mean part of the velocity field we are left with the fluctuating velocity field $u'(x)$. If the mean part is removed correctly (according to the Taylor’s theory applied here), the

The Cryosphere Discuss., doi:10.5194/tc-2015-233, 2016
Manuscript under review for journal The Cryosphere
Published: 26 January 2016

fluctuating velocities should be symmetrically distributed around zero. This is the case in our results (not shown), meaning that one can directly look at the speed (i.e., norm of the velocity) without losing information. The PDFs of the fluctuating speeds are plotted in Figure 7 with the Gaussian and exponential fits indicated for reference. We clearly see the fluctuating speeds of the IABP buoy data follow an exponential distribution with a mean equal to 6.9 cm s^{-1}. It is important to note here that the data follow an exponential distribution instead of a Gaussian distribution, as expected in fully developed turbulence (Batchelor, 1960; Frisch, 1995) and observed in different turbulent fluids (Van Atta and Chen, 1970; Zhang et al., 2001). This means that the sea ice fluctuating speed can be much larger than a standard deviation away from the (zero) mean. However, such non-Gaussian distributions for fluctuating speeds are also observed for oceanic surface currents during energetic events associated with large organised structures such as jets and vortices. Such a signature for sea ice may indicate that sea ice dynamics are dominated by the passage of large perturbations over the Arctic, whereas less energetic features have less impact on sea ice motion. This selective sensitivity to energetic events may be related to the intrinsic properties of solids associated with threshold mechanics. This seems to be supported by the fact that for weaker seasonal sea ice, the observed fluctuating velocities rather follow Gaussian statistics (Lukovich et al., 2011).

The fluctuating speeds from TOPAZ are too high on average (by about 30%) with a mean value equal to 8.97 cm s^{-1}, and their statistics do not follow an exponential distribution, hence missing the highest values of observed fluctuating speed. The fluctuating speeds from neXtSIM are slightly too low (by about 10%) with a mean value equal to 6.14 cm s^{-1} and follow an exponential distribution within the range 0 to 30 cm s^{-1}. The neXtSIM model also misses the highest values of observed sea ice fluctuating speed. The differences between the performances of the two models might come from the different rheologies, but also from the differences in the initial conditions and external forcings that are used. For example the too thin ice pack of TOPAZ at the onset of the freezing season may contribute to the overestimation of the winter drift (Rampal et al., 2011; Ólason and Notz, 2014) and could be more prone to have fluctuating speeds following a Gaussian distribution as discussed by Lukovich et al. (2011). The forcings are also not the same since the atmospheric reanalysis ASR-interim, used here to force neXtSIM, has higher spatial and temporal resolution than ERA-interim, used here to force TOPAZ. Another difference to be notified is the fact that the results of TOPAZ presented here come from a free run with no data assimilation whereas the results of neXtSIM are produced with the ocean forcing of the TOPAZ reanalysis including data assimilation. To find and explain the origins of the models performances is out of scope of the present paper and would require a dedicated analysis. However, as the forcing fields and the rheology used in TOPAZ are widely used in the sea ice modelling community, we expect the performances shown here by the TOPAZ system as a reasonable reference of most of the available coupled ocean-sea ice forecasting platforms.

Using the fluctuating part, $\mathbf{u}'$ of the velocity we calculate the fluctuating displacement components r'_x and r'_y, see Equation 18, and the norm r' of the fluctuating displacement. By analysing

The Cryosphere Discuss., doi:10.5194/tc-2015-233, 2016
Manuscript under review for journal The Cryosphere
Published: 26 January 2016

the characteristics of the norm we quantify how the distance between any particular trajectory and the mean trajectory evolves through time. To increase the robustness and statistical significance of our analysis, we artificially increase the number of buoy trajectories by splitting each trajectory into 35-day segments starting every 12 hours, i.e. every time a new buoy position along-track is available. By doing so, we make sure that the variance of the fluctuating velocities $\langle u'^2(t)\rangle$, where t here goes from 0 to 35 days, is almost constant. We verified that for each data set the deviation of $\langle u'^2(t)\rangle$ to the mean values $\langle u'^2\rangle$ is maximum of about 10%.

Figure 8 shows the evolution of the norm of the fluctuating displacement for every tenth segments retrieved from the IABP trajectories for the winter periods from 1979 to 2011. The dashed red line indicates the distance corresponding to 3 standard deviations of the fluctuating displacement. The standard deviation of the fluctuating displacement is the square root of $\langle r'^2(t)\rangle$, which is defined as

$$\langle r'^2(t)\rangle = \langle r'^2_x(t) + r'^2_y(t)\rangle. \quad (19)$$

The standard deviation of the fluctuating displacement may be a crucial piece of information for the planning of a recovery operation in a case of drifting oil or pollutant that is trapped or attached to the ice, as it gives an estimate of how the size of the searching area around the predicted mean drift should increase through time, in a statistical sense. If an operator can only trust the mean drift, which is the case for forecast longer than a few days, and if the size of the polluted ice is so small that it can be considered as a single particle (i.e. one can assume no relative dispersion of the pollutant), the searching area could be defined as a circular region with a radius depending on the standard deviation of the fluctuating displacement. We verified that about 68.9%, 95.9% and 99.6% of the fluctuating displacements are smaller than 1, 2 and 3 standard deviations, which means that the fluctuating displacement distribution is in the Gaussian attraction basin. Another way of representing the same information is to draw the relative displacement as if seen from the mean drift (see bottom panel of Figure 8). In this example, the searching radius (defined here as equal to 3 standard deviations) should be about 87 km after 5 days (corresponding to a surface area of 24000 km^2), and about 206 km after 30 days (corresponding to a surface area of 134000 km^2). As the mean speed and deformation in the Central Arctic are increasing (Rampal et al., 2009a), we may expect higher values for recent and coming years.

Another way of analysing the results is to look at the variance of the fluctuating displacement, $\langle r'^2(t)\rangle$, as a function of time (see Figure 9). This variance is sometimes called “dispersion" or “spread" around the trajectory given by the mean drift. In this paper, we rather use the term “single particle dispersion" or "absolute dispersion" to mark the difference with the relative dispersion, which indicates how the distance between two particles evolves through time. In these log-log plots the two diffusion regimes are indicated by the dashed lines showing the slope of the initial “ballistic" regime where the displacement grows with t^2, $\langle r'^2(t)\rangle \sim t^2$, and the later “Brownian" regime where the displacement grows with t, $\langle r'^2(t)\rangle \sim t$, as in the Taylor (1921) turbulent diffusion theory. The time scale at which the regime transition occurs corresponds to the integral time scale, Γ which is

The Cryosphere Discuss., doi:10.5194/tc-2015-233, 2016
Manuscript under review for journal The Cryosphere
Published: 26 January 2016

estimated as described in section 3.2.1. The value of Γ is equal to 1.4 days for the IABP data for the full winter data set, which is a value similar to the one found by Rampal et al. (2009b). For comparison, for surface ocean drift the integral times range from 1 day to 4.5 days, depending on the location (i.e., near coasts, or in the open ocean). For the atmosphere, typical integral times at altitudes lower than 300 m are five orders of magnitude smaller than for the one found for sea ice.

On the left panel, we also indicate with dotted lines the two asymptotic solutions for $\langle r'^2(t)\rangle$ for $t << \Gamma$ (from Eq. 6) and for $t >> \Gamma$ (from Eq. 7) where the constant α is neglected). These equations only depend on $\langle u'^2\rangle$ and Γ, which are given in Table 1, meaning that one can use them to estimate the variance (and then the standard deviation and searching radius as explained above) for any time t.

The right panel of Fig. 9 shows the evolution of the fluctuating displacement variance for the observed and simulated trajectories for the winters 2007-2010. The change in the slope is well reproduced by the two models, meaning that the difference between the EVP sea ice rheology used by the sea ice model of TOPAZ and the EB rheology used in neXtSIM is not discriminatory this time. However, the magnitude of the diffusion is largely overestimated with TOPAZ. This overestimation is reflected in the diffusivity parameter computed from equation 10 (see Table 1), which is almost twice as large for TOPAZ than for both neXtSIM and the observations.

If we compare diffusion properties of sea ice to diffusion properties of passive tracers in the ocean, we see that the diffusive memory, i.e. the integral time scale Γ, as well as the absolute diffusivity K are of the same order of magnitude. Using ocean drifters in the North Atlantic, Zhang et al. (2001) calculated that $\Gamma = 1.5 - 2.5$ days and $K = 1 - 7 \times 10^3\,\mathrm{m^2\,s^{-1}}$ while Poulain and Niiler (1989) calculated that $\Gamma = 4 - 5$ days and $K \sim 4 \times 10^3\,\mathrm{m^2\,s^{-1}}$ for surface drifters in the Californian Current System.

The values of diffusivity given here above are mean values over the Central Arctic, but the magnitude of the fluctuating displacements could highly vary from one region to the others. To investigate the regional distribution of the fluctuating displacements, we compute the diffusivity fields (see Figure 10). This analysis shows that in addition to the mean diffusivity the neXtSIM model also represents very well its spatial variability, with rather low diffusivity values along the Canadian Arctic Archipelago (i.e. up to about $0.5 \times 10^3\,\mathrm{m^2 s^{-2}}$) and larger values in the East Siberian Sea and in Beaufort Sea. We computed the correlation coefficient between the diffusivity map obtained from observations and those obtained from TOPAZ and neXtSIM, and found 0.7 and 0.85, respectively. One should note that the diffusivity fields could, for example, be used to evaluate the fluctuating displacement variance for $t >> \Gamma$ by using the relationship $\langle r'^2(t)\rangle = 2Kt$, which in turn could be used to estimate the searching radius in case of pollutant spill in ice-covered waters as $r_\mathrm{s} = 3\sqrt{\langle r'^2(t)\rangle}$.

The Cryosphere Discuss., doi:10.5194/tc-2015-233, 2016
Manuscript under review for journal The Cryosphere
Published: 26 January 2016

5 Conclusions

Homogeneous and stationary sea ice drift fields can be defined from Lagrangian trajectories by using averaging scales equal to $L = 400\,\mathrm{km}$ and $T = 5.5$ months for winter, and $L = 200\,\mathrm{km}$ and $T = 2.5$ months for summer. The mean drift presents an important inter-annual variability with varying magnitude and position of two main features, the Beaufort Gyre and the Transpolar drift. The mean drift velocities in winter in the Central Arctic have a mean value of about $2.5\,\mathrm{cm\,s^{-1}}$ (i.e., about $2.1\,\mathrm{km\,day^{-1}}$) for the period 2007-2010 and follow an exponential distribution, meaning that values much larger than the mean may be encountered. The mean drift could be used to predict trajectories on time scales of several weeks and months.

The fluctuating velocities are isotropic and follow an exponential distribution with a mean value of about $7\,\mathrm{cm\,s^{-1}}$ (i.e., about $6\,\mathrm{km\,day^{-1}}$) for the winters 2007-2010. The ensemble average auto-correlation function crosses the zero axis at around 6 days, meaning that fluctuating velocities are uncorrelated for larger time scales. Fluctuating displacements may be considered as Gaussian since about 68.9%, 95.9% and 99.6% of the fluctuating displacements are smaller than 1, 2 and 3 standard deviations. If we are looking for the position of a single ice particle, the searching area around the position predicted by the mean drift could be defined as a circular region with a radius equal to 3 standard deviations of the fluctuating displacement. On average for the winter periods 1979-2011, we find that the searching radius should be about 87 km after 5 days (corresponding to a surface area of $24000\,\mathrm{km^2}$), and about 206 km after 30 days (corresponding to a surface area of $134000\,\mathrm{km^2}$). This of course may vary from one region to another, depending on the local dynamical regime of sea ice, e.g. like in the Beaufort Sea, the transpolar drift area and the marginal ice zone. Also, the size of the searching area may have varied over time, with expected higher values for recent and coming years due to the observed increasing mean sea ice speed and deformation in the Arctic.

The fluctuating displacement variance evolves following two regimes of diffusion as a function of the time scale considered: a “ballistic" regime for time scales shorter than about 1 day and for which the variance grows with t^2, and a “Brownian" regime for time scales much larger than 1 day and for which the variance grows with t. The evolution of the variance can be fully described by two parameters $\langle u'^2 \rangle$ (the fluctuating velocity variance) and Γ (the integral time scale). For example, for very large t, the variance can be estimated as $\langle r'^2(t) \rangle = 2Kt$, where K, the absolute diffusivity, is computed as $K = \langle u'^2 \rangle \Gamma$. For the winters 1979-2011, K is estimated as equal to $1.2 \times 10^3\,\mathrm{m^2 s^{-2}}$, which is in the range of values found in the literature for sea ice and oceanic surface. Diffusivity is not constant within the Arctic basin, with significantly lower values along the Canadian Arctic Archipelago. One should also note that the diffusivity fields or constant can be used along with the mean drift into an advection-diffusion equation or with Lagrangian stochastic models to estimate the probability for a particle to be in a given position after a given time.

Sea ice-ocean models should be able to represent correctly the inter-annual variability, but also the statistical and geographical distribution of the mean drift, which seems clearly not to be the case for

The Cryosphere Discuss., doi:10.5194/tc-2015-233, 2016
Manuscript under review for journal The Cryosphere
Published: 26 January 2016

the TOPAZ system. The mean velocities in TOPAZ are on average 40% too high, follow a Gaussian instead of an exponential distribution and do not represent correctly the circulation patterns in Arctic. On another hand the neXtSIM model performs better, in particular in terms of statistical and spatial distributions.

The fluctuating velocities in the TOPAZ model are too high on average and follow a Gaussian distribution, whereas observations follow an exponential distribution. The fluctuating velocities in the neXtSIM model are slightly lower on average compared to observations, but their distribution follows an exponential model like the observations. The fluctuating velocity variance is too large in the TOPAZ model, leading to an absolute diffusivity almost twice as large as the one estimated from the observations and from the neXtSIM model. The differences in performance of the two modelling platforms might partly result from the fundamental difference in their sea ice dynamical framework and in particular the rheology they use. They may also come from differences in the initial conditions (in particular the initial thickness field) and forcings fields each model used. However, one should still remind that despite these differences both these models are finely tuned with respect to their configuration (atmospheric forcing, initial conditions, etc...) in order to get the best performance overall, and with regard to sea ice drift in particular.

The Cryosphere Discuss., doi:10.5194/tc-2015-233, 2016
Manuscript under review for journal The Cryosphere
Published: 26 January 2016

Appendix A: Link with passive tracer trajectory modelling

Both the mean and the fluctuating parts of the motion are important information for passive tracer trajectory modelling in ice covered areas. The mean drift indicates the general direction that will be followed by the ice for the next weeks ($T = 165$ days for the central Arctic in winter) and could be correctly provided by medium-resolution seasonal prediction models or retrieved from sea ice drift observation data sets by averaging sea ice drift over the last $T/2$ period. The fluctuating part may be analysed to indicate how a particular trajectory may differ from the trajectory predicted by the mean drift.

When the characteristics of turbulent fluids are reproduced in a particular medium, the information on the mean drift and absolute diffusivity can directly be used to predict the trajectory of any passive tracer moving with this medium (LaCasce, 2008). Continuous passive tracer models generally use the classical advection-diffusion equation

$$\frac{\partial C}{\partial t} + \bar{\mathbf{u}} \cdot \nabla C = \nabla \cdot (K \nabla C), \tag{A1}$$

where $\bar{\mathbf{u}}$ is the mean velocity field defined with the right averaging scales (L and T) and K is the corresponding diffusivity field or constant parameter. This equation can be used in two cases. If the release of the passive tracer has occurred in a so short time and over a so small area that the tracer can be viewed as a single particle with a unique position at a given time, then the advection-diffusion equation can be viewed as a stochastic differential equation where C describes the probability for the particle to be in a given position after a given time. If the tracer is released (i.e., via a source term in equation A1) during a long period (typically T) or over a large area (typically L), then C can be viewed as the passive tracer concentration, or in the two-dimensional case as the volume of pollutant per surface area (Monin and Yaglom, 1975).

Discrete passive tracer models may also be used. In this case, the displacement dx_i in the i direction needs to be defined for each independent objects. The simplest approach, known as the “random walk" model, neglects the transition between “ballistic" and the “Brownian" regimes and simply defines the dx_i by

$$dx_i = \bar{u}_i dt + \sqrt{2}\sqrt{\langle u_i'^2 \rangle} dw_i, \tag{A2}$$

where u_i' is the fluctuating velocity in the i direction and dw_i is a Weiner process. This equation is strictly equivalent to the advection-diffusion equation of continuous models.

To also represent the “ballistic" regime, a more complex approach consists in applying the stochastic term on the evolution of the velocity, leading to the following set of equations:

$$dx_i = (u_i + \bar{u}_i) dt \tag{A3}$$

$$du_i = -\frac{1}{T_i} u_i dt + \sqrt{\frac{2}{T_i}} \sqrt{\langle u_i'^2 \rangle} dw_i. \tag{A4}$$

Despite its greater complexity, this model is not suitable for all applications, as it assumes that particle velocities are uncorrelated in space.

The Cryosphere Discuss., doi:10.5194/tc-2015-233, 2016
Manuscript under review for journal The Cryosphere
Published: 26 January 2016

Such approaches can be used to study the evolution of passive tracer in a medium only if it exhibits the same characteristics as molecular diffusion (particles velocities are uncorrelated in space). When this condition is not satisfied, which is indeed the case for sea ice and the ocean surface, the passive tracer model has to be included or directly forced by a dynamical model simulating the motion fields. The most used approach in passive tracer trajectory modelling (e.g. for oil spill modelling) consists in setting a bunch of virtual floats in the region of interest and defining their motion as a function of the sea ice drift, wind and oceanic currents simulated by dynamical models, using an off-line or in-line tracking system similar to the ones presented in Section 2.2 and 2.3. However before using such dynamical models for passive tracer modelling, one should verify that these models reproduce well the mean drift and the fluctuating part of the motion, and the diffusion analysis presented in Section 3 is a powerful tool to perform such a validation.

Acknowledgements. We would like to acknowledge L. Bertino, J. Xie and P. Griewank for interesting discussions and their contribution to the development of TOPAZ and neXtSIM. We also thank T. Williams for his help improving the manuscript. This work was supported by fundings from the Oil and Gas Producers (OGP), TOTAL E&P and the Norwegian Council of Norway.

The Cryosphere Discuss., doi:10.5194/tc-2015-233, 2016
Manuscript under review for journal The Cryosphere
Published: 26 January 2016

References

Batchelor, G. K.: The theory of homogeneous turbulence, Students' edition. By G. K. Batchelor. Cambridge Monographs on Mechanics and Applied Mathematics. Cambridge (University Press), 1959. Pp. xi, 197; 28 Figures; 18s. 6d, Quarterly Journal of the Royal Meteorological Society, 86, 291–291, 1960.

Bleck, R.: An oceanic general circulation model framed in hybrid isopycnic-Cartesian coordinates, Ocean Modelling, 4, 55 – 88, doi:http://dx.doi.org/10.1016/S1463-5003(01)00012-9, 2002.

Bouillon, S. and Rampal, P.: Presentation of the dynamical core of neXtSIM, a new sea ice model, Ocean Modelling, 91, 23–37, 2015.

Bromwich, D. H., Wilson, A. B., Bai, L.-S., Moore, G. W. K., and Bauer, P.: A comparison of the regional Arctic System Reanalysis and the global ERA-Interim Reanalysis for the Arctic, Quarterly Journal of the Royal Meteorological Society, pp. n/a–n/a, doi:10.1002/qj.2527, http://dx.doi.org/10.1002/qj.2527, 2015.

Colony, R. and Thorndike, A. S.: Sea ice motion as a drunkard's walk, J. Geophys. Res., 90, 965–974, 1985.

Drange, H. and Simonsen, K.: Formulation of air-sea fluxes in the ESOP2 version of MICOM, Tech Rep. 125, Tech. rep., NERSC, Bergen, Norway, www.nersc.no, 1996.

Drozdowski, A., Nudds, S., Hannah, C. G., Niu, H., Peterson, I., and Perrie, W.: Review of Oil Spill Trajectory Modelling in the Presence of Ice, Tech. rep., Canadian Tech. Rep. Hydrogr. Ocean Sci. 274, 2011.

Frisch, U.: Turbulence: The Legacy of A. N. Kolmogorov, Cambridge University Press, U.K., 1995.

Hunke, E. C. and Dukowicz, J. K.: An elastic-viscous-plastic model for sea ice dynamics, J. Phys. Ocean., 27, 1849–1867, 1997.

Hunke, E. C. and Lipscomb, W. H.: CICE model Ver. 4.1 Documentation, pp. 1–76, 2010.

Jiang, G.-S. and Shu, C.-W.: Efficient implementation of weighted ENO schemes, Journal of Computational Physics, 228, 202–228, doi:10.1006/jcph.1996.0130, 1995.

Kaleschke, L., Lüpkes, C., Vihma, T., Haarpaintner, J., Bochert, A., Hartmann, J., and Heygster, G.: SSM/I Sea Ice Remote Sensing for Mesoscale Ocean-Atmosphere Interaction Analysis, Canadian Journal of Remote Sensing, 27, 526–537, 2001.

LaCasce, J. H.: Statistics from Lagrangian observations, Prog. Oceanogr., 77, 1–29, 2008.

Lukovich, J. V., Babb, D. G., and Barber, D. G.: On the scaling laws derived from ice beacon trajectories in the southern Beaufort Sea during the International Polar Year - Circumpolar Flaw Lead study, 2007–2008, J. Geophys. Res., 116, C00G07, 2011.

Lukovich, J. V., Hutchings, J. K., and Barber, D. G.: On sea-ice dynamical regimes in the Arctic Ocean, Annals of Glaciology, 56, 323–331, 2015.

Monin, A. S. and Yaglom, A. M.: Statistical Fluid Mechanics, vol. II, MIT Press, Cambridge, MA, 1975.

Ólason, E. and Notz, D.: Drivers of variability in Arctic sea-ice drift speed, Journal of Geophysical Research: Oceans, 119, 5755–5775, doi:10.1002/2014JC009897, http://dx.doi.org/10.1002/2014JC009897, 2014.

Poulain, P.-M. and Niiler, P. P.: Statistical analysis of the surface circulation in the California Current System using satellite-tracked drifters, J. Phys. Ocean., 19, 1588–1603, 1989.

Rampal, P., Weiss, J., Marsan, D., Lindsay, R., and Stern, H.: Scaling properties of sea ice deformation from buoy dispersion analysis, Journal of Geophysical Research: Oceans, 113, n/a–n/a, doi:10.1029/2007JC004143, http://dx.doi.org/10.1029/2007JC004143, c03002, 2008.

The Cryosphere Discuss., doi:10.5194/tc-2015-233, 2016
Manuscript under review for journal The Cryosphere
Published: 26 January 2016

Rampal, P., Weiss, J., and Marsan, D.: Positive trend in the mean speed and deformation rate of Arctic sea ice, 1979-2007, Journal of Geophysical Research: Oceans, 114, n/a–n/a, doi:10.1029/2008JC005066, http://dx.doi.org/10.1029/2008JC005066, c05013, 2009a.

Rampal, P., Weiss, J., Marsan, D., and Bourgoin, M.: Arctic sea ice velocity field: General circulation and turbulent-like fluctuations, Journal of Geophysical Research: Oceans, 114, C10 014, 2009b.

Rampal, P., Weiss, J., Dubois, C., and Campin, J.-M.: IPCC climate models do not capture Arctic sea ice drift acceleration: Consequences in terms of projected sea ice thinning and decline, Journal of Geophysical Research: Oceans, 116, n/a–n/a, doi:10.1029/2011JC007110, http://dx.doi.org/10.1029/2011JC007110, c00D07, 2011.

Rampal, P., Bouillon, S., Ólason, E., and Morlighem, M.: neXtSIM: a new Lagrangian sea ice model, The Cryosphere Discussions, 9, 5885–5941, doi:10.5194/tcd-9-5885-2015, http://www.the-cryosphere-discuss.net/9/5885/2015/, 2015.

Sakov, P., Counillon, F., Bertino, L., Lisæter, K. A., Oke, P., and Korablev, A.: TOPAZ4: An ocean sea ice data assimilation system for the North Atlantic and Arctic, Ocean Sci., 8, 633–662, doi:10.5194/osd-9-1519-2012, 2012.

Schweiger, A., Lindsay, R., Zhang, J., Steele, M., Stern, H., and Kwok, R.: Uncertainty in modeled Arctic sea ice volume, Journal of Geophysical Research: Oceans, 116, n/a–n/a, doi:10.1029/2011JC007084, http://dx.doi.org/10.1029/2011JC007084, c00D06, 2011.

Semtner, A. J.: A model for the thermodynamic growth of sea ice in numerical investigations of climate, J. Phys. Ocean., 6, 379–389, 1976.

Spreen, G., Kaleschke, L., and Heygster, G.: Sea ice remote sensing using AMSR-E 89-GHz channels, Journal of Geophysical Research: Oceans, 113, n/a–n/a, doi:10.1029/2005JC003384, http://dx.doi.org/10.1029/2005JC003384, c02S03, 2008.

Taylor, G. I.: Diffusion by Continuous Movements, Proceedings of The London Mathematical Society, s2-20, 196–212, doi:10.1112/plms/s2-20.1.196, 1921.

Thomas, D.: The quality of sea ice velocity estimates, J. Geophys. Res., 104, 13 627, 1999.

Thorndike, A. S.: Diffusion of sea ice, J. Geophys. Res., 91, 7691–7696, 1986.

Van Atta, C. W. and Chen, W. Y.: Structure functions of turbulence in the atmospheric boundary layer over the ocean, Journal of Fluid Mechanics, 42, 689, 1970.

Zhang, H., Prater, M. D., and Rossby, T.: Isopycnal Lagrangian statistics from the North Atlantic Current RAFOS float observations, J. Geophys. Res., 106, 13 817, 2001.

Zhang, J. and Rothrock, D.: Modeling global sea ice with a thickness and enthalpy distribution model in generalized curvilinear coordinates, Monthly Weather Review, 131, 845–861, 2003.

The Cryosphere Discuss., doi:10.5194/tc-2015-233, 2016
Manuscript under review for journal The Cryosphere
Published: 26 January 2016

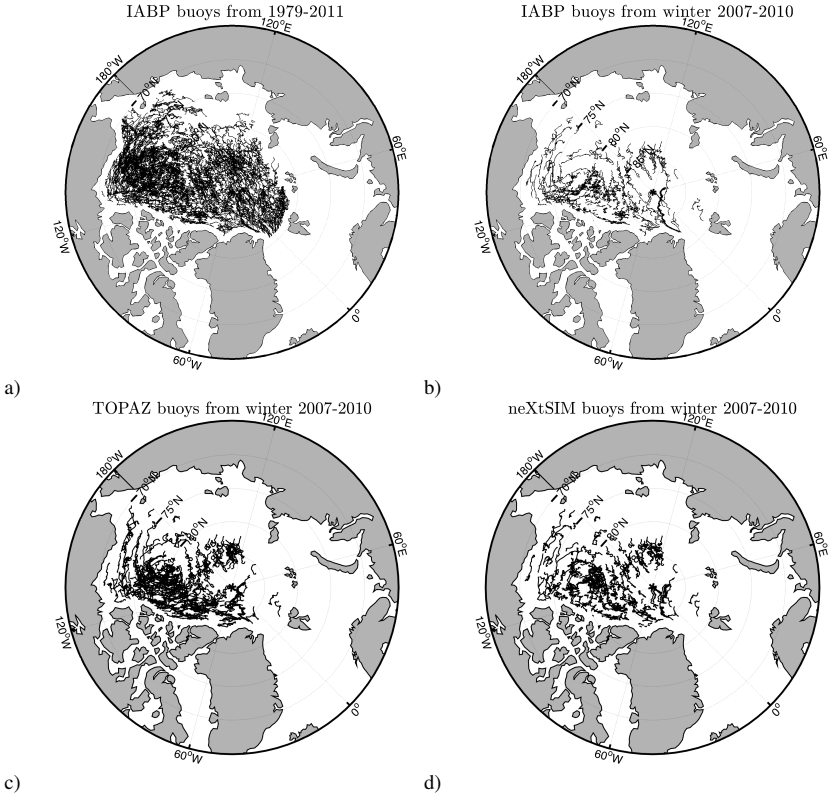

Figure 1. Buoy tracks from a) the IABP dataset for 1979 to 2011, b) the IABP dataset for winter seasons 2007 to 2010, c) the TOPAZ simulations for winter seasons 2007 to 2010, and d) the neXtSIM simulations for winter seasons 2007 to 2010.

The Cryosphere Discuss., doi:10.5194/tc-2015-233, 2016
Manuscript under review for journal The Cryosphere
Published: 26 January 2016

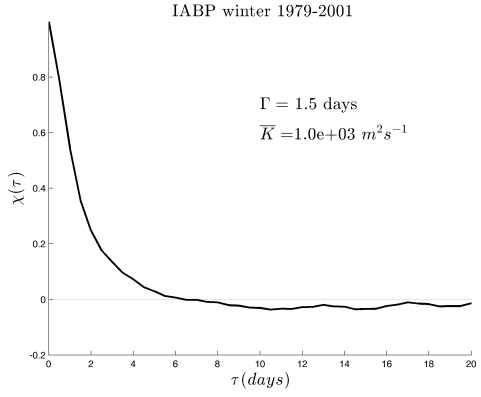

Figure 2. Ensemble averaged fluctuating velocity autocorrelation function for the IABP dataset for winter seasons 1979 to 2001. The values of the integral time scale Γ and mean horizontal diffusivity $\bar{K}$ for this particular period are indicated.

The Cryosphere Discuss., doi:10.5194/tc-2015-233, 2016
Manuscript under review for journal The Cryosphere
Published: 26 January 2016

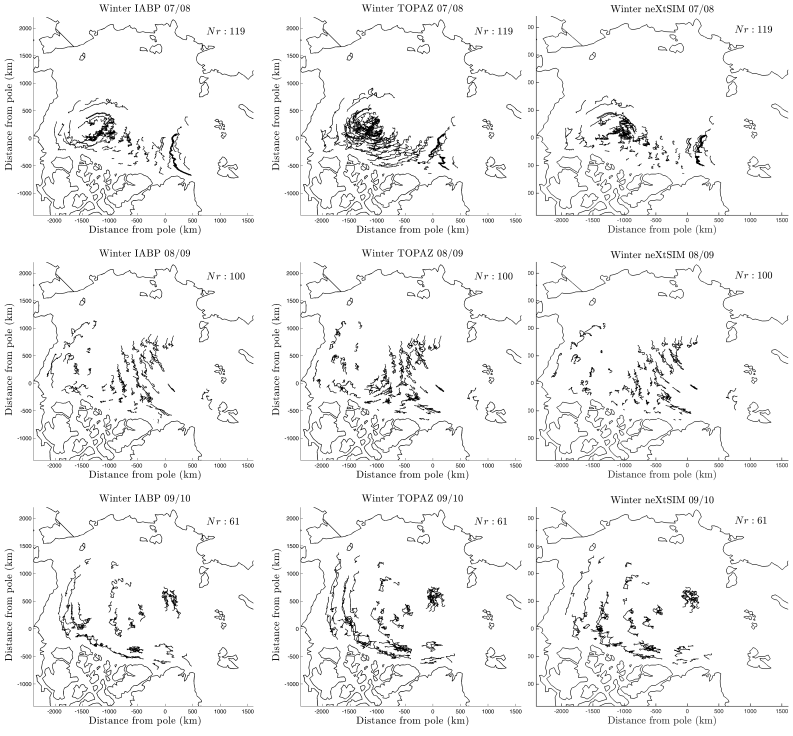

Figure 3. IABP buoys tracks (left) and their corresponding virtual tracks simulated by TOPAZ (centre) and neXtSIM (right) for the winters 2007/2008 (top), 2008/2009 (middle), and 2009/2010 (bottom).

The Cryosphere Discuss., doi:10.5194/tc-2015-233, 2016
Manuscript under review for journal The Cryosphere
Published: 26 January 2016

The Cryosphere Discussions
Open Access
EGU

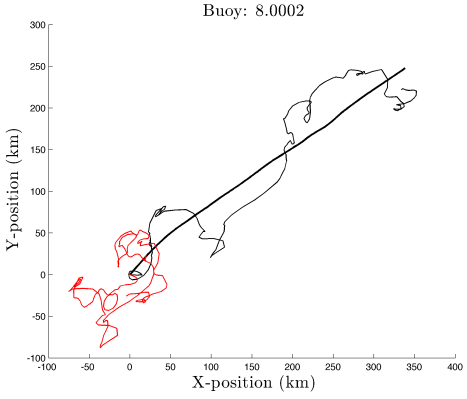

Figure 4. Trajectory of the buoy 8.0002 from the IABP dataset (thin black) partitioned into a mean (thick black) and fluctuations (red) trajectories using the method described in section 3.

The Cryosphere Discuss., doi:10.5194/tc-2015-233, 2016
Manuscript under review for journal The Cryosphere
Published: 26 January 2016

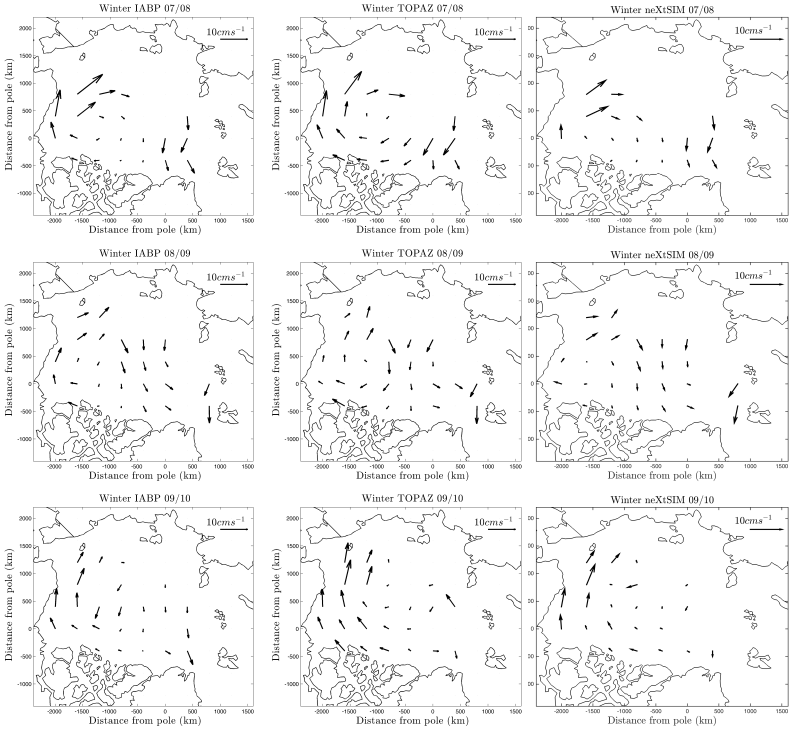

Figure 5. Mean sea ice velocity field computed from the IABP buoys dataset (left) and the corresponding floats dataset generated with TOPAZ (centre), and neXtSIM (right) for the winters 2007/2008 (top), 2008/2009 (middle), and 2009/2010 (bottom). The mean velocity vectors are shown on a 400×400 km regular grid, with coordinates $(\hat{x}, \hat{y})$. The plotted vectors are the weighted average of the mean Lagrangian velocities of the buoys located within a circle of radius $L/2$ centred on $(\hat{x}, \hat{y})$. The applied weight is $w = e^{-r^2/(2L^2)}$ where r is the distance between a given buoy position and the grid point, i.e. $r = \sqrt{(x-\hat{x})^2 + (y-\hat{y})^2}$.

The Cryosphere Discuss., doi:10.5194/tc-2015-233, 2016
Manuscript under review for journal The Cryosphere
Published: 26 January 2016

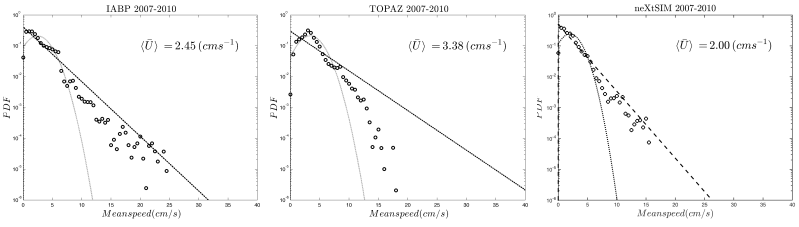

Figure 6. Probability density function of the mean speed of the IABP buoys (left), and of the corresponding virtual floats in TOPAZ (middle) and neXtSIM (right) for the period 2007-2010. The Gaussian (light grey line) and exponential (black dots) fits of the data are also indicated.

The Cryosphere Discuss., doi:10.5194/tc-2015-233, 2016
Manuscript under review for journal The Cryosphere
Published: 26 January 2016

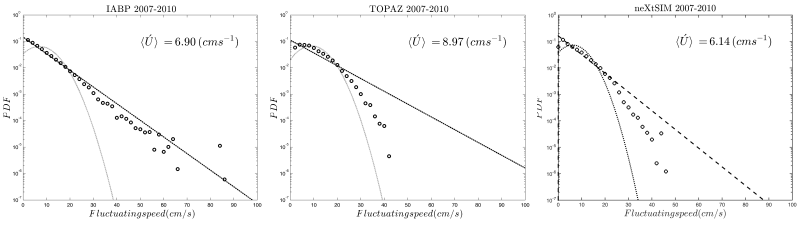

Figure 7. Probability density function of the fluctuating speed of the IABP buoys (left), and of the corresponding virtual floats in TOPAZ (middle) and neXtSIM (right) for the winter periods 2007-2010. The Gaussian (light grey line) and exponential (black dots) fits of the data are also indicated.

The Cryosphere Discuss., doi:10.5194/tc-2015-233, 2016
Manuscript under review for journal The Cryosphere
Published: 26 January 2016

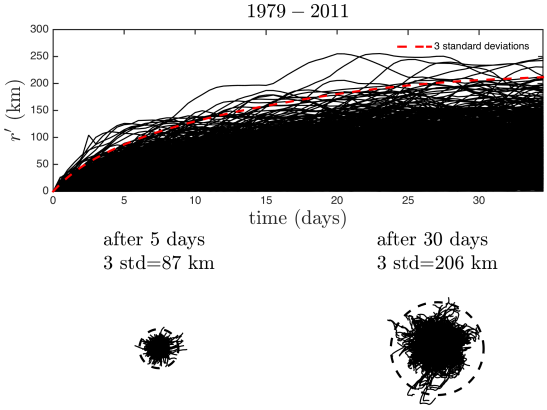

Figure 8. Time evolution of the norm of the fluctuating displacement r' for every tenth 35-days segments extracted from the IABP buoys tracks for the winters 1979-2011 (top). The dashed red line indicates 3 standard deviations of the fluctuating displacement. Fluctuating part of the buoy trajectories and estimated searching area radius after 5 and 30 days (bottom).

The Cryosphere Discuss., doi:10.5194/tc-2015-233, 2016
Manuscript under review for journal The Cryosphere
Published: 26 January 2016

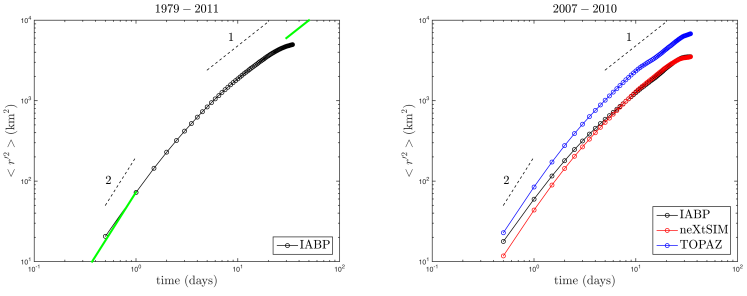

Figure 9. Ensemble mean of the variance of the fluctuating displacement $< r'^2 >$ for the winter seasons 1979-2011 (for IABP only, left panel) and 2007-2011 (for IABP, TOPAZ and neXtSIM, right panel). The dashed lines show the theoretical "ballistic" ($\langle r'^2(t) \rangle \sim t^2$) and "Brownian" ($\langle r'^2(t) \rangle \sim t$) regimes. The green lines on the left panel correspond to the equations 6 and 7 and are shown for reference.

The Cryosphere Discuss., doi:10.5194/tc-2015-233, 2016
Manuscript under review for journal The Cryosphere
Published: 26 January 2016

The Cryosphere Discussions
Open Access
EGU

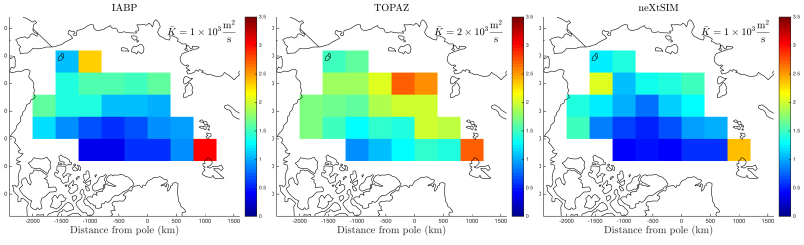

Figure 10. Mean diffusivity fields obtained from the analysis of the IABP buoys trajectories (left), TOPAZ floats trajectories (middle), and neXtSIM floats trajectories (right) for the winters 2007-2010. The local diffusivity values are shown as colours in 400×400 km boxes. Note that the mean diffusivity $\bar{K}$ averaged over the whole Arctic basin from the values shown here for each boxes is slightly different than the estimate given in Table 1 due to differences in the averaging method.

The Cryosphere Discuss., doi:10.5194/tc-2015-233, 2016
Manuscript under review for journal The Cryosphere
Published: 26 January 2016

The Cryosphere Discussions
Open Access
EGU

Table 1. This table shows the total number of floats (Nrf), the number of 35 days segments ($Nseg$), the calculated integration time scale (Γ), the variance $\langle u'^2 \rangle$ and the calculated diffusivity K for the different dataset (IABP, TOPAZ and neXtSIM) and time periods used in this study. All these Lagrangian statistics were computed following the diffusion theory of Taylor (1921) and using $L = 400$ km and $T = 165$ days as averaging scales to calculate the Lagrangian mean velocities

$Source$	$Period$	Nrf	$Nseg$	$\Gamma(day)$	$\langle \acute{u}^2 \rangle (km^2\, day^{-2})$	$K10^3 (m^2 s^{-1})$
IABP	1979-2011	1406	19110	1.4	73	1.2
IABP	2007-2010	280	3720	1.1	64	0.8
TOPAZ	2007-2010	280	3720	1.5	89	1.5
neXtSIM	2007-2010	280	3720	1.3	52	0.8